



## PAPER

Nonlinear optical response of silver trimer adsorbed *para*-aminobenzoic acid: A DFT study

## RECEIVED

23 August 2023

## REVISED

25 September 2023

## ACCEPTED FOR PUBLICATION

5 October 2023

## PUBLISHED

17 October 2023

Shradha Lakhera, Kamal Devlal and Meenakshi Rana\*

Department of Physics, School of Sciences, Uttarakhand Open University, Haldwani, 263139, Uttarakhand, India

\* Author to whom any correspondence should be addressed.

E-mail: [mrana@uou.ac.in](mailto:mrana@uou.ac.in)**Keywords:** density functional theory, *para*-aminobenzoic acid, adsorption, density functional theory, *para*-aminobenzoic acid, silver, adsorptionSupplementary material for this article is available [online](#)**Abstract**

The reported study is motivated by our previously done experimental demonstration of the optical limiting behavior of *para*-aminobenzoic acid and enhanced nonlinear optical responses of compounds with Ag<sub>3</sub> nanoparticle complex. The present study is a theoretical insight into the nonlinear optical responses of *para*-aminobenzoic acid adsorbed with Ag<sub>3</sub> trimer. The enhancement in the optical nonlinearity of the *para*-aminobenzoic acid after the adsorption of the silver trimer (Ag<sub>3</sub>) was accounted in the present study. The density functional theory was used to establish the occurrence of the intra and intermolecular charge transfer between the donor and acceptor moieties of the *para*-aminobenzoic acid and Ag<sub>3</sub> trimer. The molecular electrostatic potential surface and inter-fragment charge transfer analysis were used to establish the donor nature of the Ag<sub>3</sub> trimer, amino group, and acceptor of the carboxyl group. The absorption spectra and Fourier-transform infrared spectra were used to account for the electronic and vibrational modes. The value of first-order hyperpolarizability of *para*-aminobenzoic acid and Ag<sub>3</sub> complex was observed to increase by six times that of *para*-aminobenzoic acid. The high value of first-order hyperpolarizability shows the potential nonlinear optical activity of *para*-aminobenzoic acid adsorbed with Ag<sub>3</sub> trimer. The presented study forms a strong base for experimental demonstration of the nonlinear optical activity of the PABA and the silver nanoparticles and the experimental work will be done in the near future for the NLO responses and optical limiting activity of PABA combined with silver nanoparticles.

**1. Introduction**

The modern world is in great demand for thermodynamically stable and highly polarizable compounds that are highly applicable in optoelectronics, telecommunications, and laser industry [1, 2]. The compounds with such properties are nonlinear optical (NLO) materials and the field of technology has all been vastly assisted by the compounds with optical nonlinearity. The gradually emerging and trending fields like optical computing, 3D optical data storage, frequency generation and mixing, information processing, optical power limiting, telecommunication systems, etc, have increased the urge for NLO materials [3–5]. The desired properties of the NLO materials have been derived from different nude systems like aromatic compounds, plant phytochemicals, nitrogenated and oxygenated compounds, lanthanides, actinides, and many more [6–10]. However, the emergence of nanotechnology has given a new face to NLO as well. Literature reported so far shows that the doping of the nano-particles has given a boost to the desirable properties of the NLO materials [11]. The particles of size 10<sup>-9</sup> m are generally referred to as nanomaterials [12]. Since they are very tiny, their radius is also very small, and a small radius results in a large value of surface area to volume ratio [13]. The high value of the surface area to volume ratio leads to high chemical reactivity and polarizability of the nanomaterials [14]. Thus, the nanomaterials are found to be potent dopants for increasing the polarizability and NLO activity of the materials

[15–18]. Silver nanoparticles have been revolutionary nanoparticles and have a lot of applications in optoelectronics. A novel NHC porous organic polymer with silver nanoparticles was synthesized using a pre-coordination method, enabling simultaneous CO<sub>2</sub> capture and activation [19]. The proposed complex with silver nanoparticles served as a catalyst to convert the carbon dioxide from lime waste gas into carbonates. This remarkable application of the silver nanoparticle is proven to be a 99% successful yield [19]. There are numerous studies reported previously that account for the immensely enhanced NLO activity of the compounds after the substitution or doping of the nanoparticles. The NLO activity of 4-[(E)-2-(2,4,6-Trinitrophenyl) ethylidene] benzonitrile doped with silver nanoparticles was reported by John and his team [20]. The nonlinear transmittance of 60% was obtained for 4-[(E)-2-(2,4,6-Trinitrophenyl) ethylidene] benzonitrile+silver clusters and was employed for the applications of optical limiting as well as green light emitting diode [20]. The NLO activity of the single crystal of 2-methyl-5-nitroaniline was calculated with and without the doping of the silver nanoparticles [21]. The nonlinear transmittance of 72% and 92% for 2-methyl-5-nitroaniline without silver nanoparticles and with nanoparticles was obtained [21]. The NLO activity of the pyrene with a silver solution was reported by U. R. Felscia [22]. N, N-dimethyl urea ninhydrin, and L-histidine were some more systems where the optical nonlinearity was observed to be escalated [23, 24]. Along with the organic systems, the doping of silver nanoparticles has also given a medium to the optical nonlinearity of inorganic systems. Aboalhassan and his team identified that the optical nonlinearity of meso-terakis (4-sulfonate phenyl) porphyrin was increased after the doping of silver nanoparticles and the property of fluorescence quenching was also noticed [25].

Apart from the experimental demonstrations, the computational investigations for the enhanced NLO activity of the organic donor–acceptor-rich systems with doped/adsorbed silver nanoparticles have been previously performed. The reports that we have previously presented by calculating the NLO activity of Pentacece-2,5-dione after the adsorption of gold and silver trimer were very promising [26]. For probe pentacene-2,5-dione, the value of hyperpolarizability was very low about  $0.000181 \times 10^{-30}$  esu, but the complex formed after the adsorption of Ag<sub>3</sub> trimer with pentacene-2,5-dione gave an extremely enhanced value of hyperpolarizability of  $2057.26 \times 10^{-30}$  esu [26]. We have also explored the values of dipole moment, polarizability, and first-order hyperpolarizability of 2,9-dimethyl quinacridone using density functional theory (DFT) tools. The results are found to be highly satisfactory. The values of first-order hyperpolarizability before and after the adsorption of the Ag<sub>3</sub> trimer were calculated as  $0.001416 \times 10^{-30}$  and  $1066.85 \times 10^{-30}$  esu [27]. The same kind of combined computational and experimental study on the silver nanoparticle extracted using honey combined with an Oxytetracycline molecule was performed by Alejandro González Fá and the team [28]. The vibrational spectra discussed in the reference article show the adsorption of oxytetracycline on the silver nanoparticle. Similar kinds of other studies are present in the literature which has been a big motivation for pursuing this study. After carrying out experiments for *para*-aminobenzoic acid (PABA) and getting satisfactory results, the investigation of the NLO activity of PABA+Ag<sub>3</sub> is predicted to give satisfactory results too.

The present study is the extension of our previously reported work in which we have investigated the NLO characteristics of probe PABA [29]. The clusters formed from the adsorption of Ag<sub>3</sub> over the organic systems like pentacene-2,5-dione and 2,9-dimethyl quinacridone investigated previously were very promising and gave satisfying results [26, 27]. Thus, PABA+Ag<sub>3</sub> is taken as the target complex for checking for its NLO activity. A significantly high NLO activity is expected from a complex of PABA+Ag<sub>3</sub>. This novel-designed complex will be a combination of organic compound and nanoparticle. This combination can be used for different optoelectronic and NLO applications and can be used as a basis study for performing experimental studies. The present study aims to investigate the NLO activity of the PABA+Ag<sub>3</sub> complex using DFT tools. Koopman's equation was used for calculating the reactivity parameters and molecular electrostatic potential surfaces (MEP) were used to identify the reactive moieties. Inter-fragment charge transfer (IFCT) analysis was done to predict the quantitative charge transfer. Computational absorption and Fourier Transform-Infrared (FT-IR) spectroscopy were accounted for analyzing the electronic and vibrational properties. The polarizability and hyperpolarizability parameters were used to predict the NLO activity of the complex.

## 2. Materials and methods

DFT was taken as the basic computational tool for the present study. The structure of PABA was downloaded from PubChem (<https://pubchem.ncbi.nlm.nih.gov/>). PABA is an organic compound also known as vitamin B. It is used in sun screening agents and also used in some therapeutic skin disorders. According to PubChem toxicological information and carcinogenicity evidence, PABA is found to be non-carcinogenic to humans and is also used in many drugs. All the necessary quantum chemical calculations to obtain the stable configuration of the complex were performed using Gaussian software packages (<https://gaussian.com/>) with Gauss view as the graphic user interface (<https://gaussian.com/gaussview6/>) [30]. Basis set B3LYP/6-311++G(d,p) was used for the ground state optimization of the probe PABA. The mentioned set of hybrid functionals is mostly used for

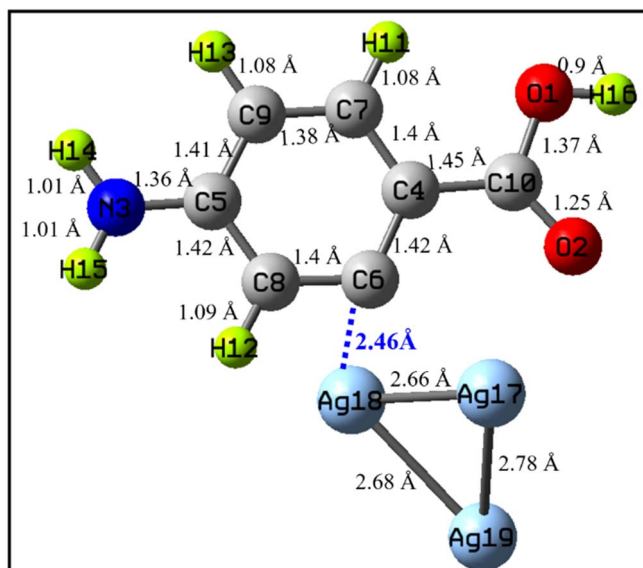


Figure 1. Optimized geometry of PABA interacted with  $\text{Ag}_3$  cluster.

optimizing the organic systems. After the optimization of probe PABA with B3LYP/6-311++G(d,p) [31, 32], the silver trimer ( $\text{Ag}_3$ ), was drawn using the builder tool at a distance of 3 Å. This intermolecular distance is considered an ideal distance to study the nature of adsorption between the adsorbent (suppose PABA) and adsorbate ( $\text{Ag}_3$  in our case). Similar geometry optimization was performed for PABA+ $\text{Ag}_3$  as before but with a B3PW91/cc-pVDZ set of functions. These hybrid functionals are considered far easier and more accurate in case the structure consisting of metallic atoms [26, 27]. Thus, the required parameters like dipole moment, global reactivity descriptors, MEP surface, counterplots, the density of states, etc, were recovered using the optimized geometry of the PABA+  $\text{Ag}_3$  complex. Global reactivity descriptors were calculated using Koopman's set of equations [33]. The integral equation formalism-polarizable continuum model (IEFPCM) model with the self-consistent reaction field (SCRf) method was used for reporting the behavior of the complex in different solvents like water, methanol, dimethyl formamide (DMF), and dimethyl sulfoxide (DMSO). The dipole moment, global reactivity descriptors, and the NLO parameters were compared for all the considered solvents. Time-dependent density functional theory (TD-DFT) was employed to get the absorption spectra of the PABA+  $\text{Ag}_3$  complex. The polar calculations were performed with the same set of functionals for obtaining the values of polarizability and hyperpolarizability. The mathematical expressions that are followed for calculating the NLO parameters and all the other tools and techniques are similar to those used in the reference study [26, 27, 29, 34].

### 3. Results and discussion

#### 3.1. Structural and adsorption analysis

The optimized geometry of PABA+ $\text{Ag}_3$  was obtained to the true local minima. After optimization, the  $\text{Ag}_3$  trimer was at a distance of 2.46 Å from the PABA. The optimized bond lengths of PABA+ $\text{Ag}_3$  are indicated in figure 1. Higher bond lengths were observed for the bonds associated with the -COOH group. The bonds joining the  $\text{Ag}_3$  trimer were observed with the highest bond length of 2.66 Å (18Ag-19Ag), 2.782 Å (17Ag-19Ag), and 2.685 Å (18Ag-19Ag). The quantitative changes that will be generated in the system will predict the NLO characteristics of the PABA+ $\text{Ag}_3$  complex. The high bond length provides suitable conditions for the generation of the charge cloud [35]. Basically, the long bond lengths tend to get alternate contractions and stretch when kept in higher magnitudes of electric fields. As we are dealing with the optical nonlinearity of the proposed complex, the field provided to the system will be of high magnitude [36]. Thus, the larger bond lengths of the  $\text{Ag}_3$  trimer result in generating the charge cloud and show the active participation of the trimer to participate in inter and intramolecular interactions and contribute to increasing the NLO activity of the PABA+ $\text{Ag}_3$  complex.

#### 3.2. Molecular orbitals analysis

Frontier molecular orbitals or called global reactivity descriptors were calculated for the PABA+ $\text{Ag}_3$  complex (in gas phase and in the different solvents) and were further compared with the FMO parameters of probe PABA (table 1). The band gap of probe PABA in the gas phase was calculated as 4.775 eV. This value was found to be

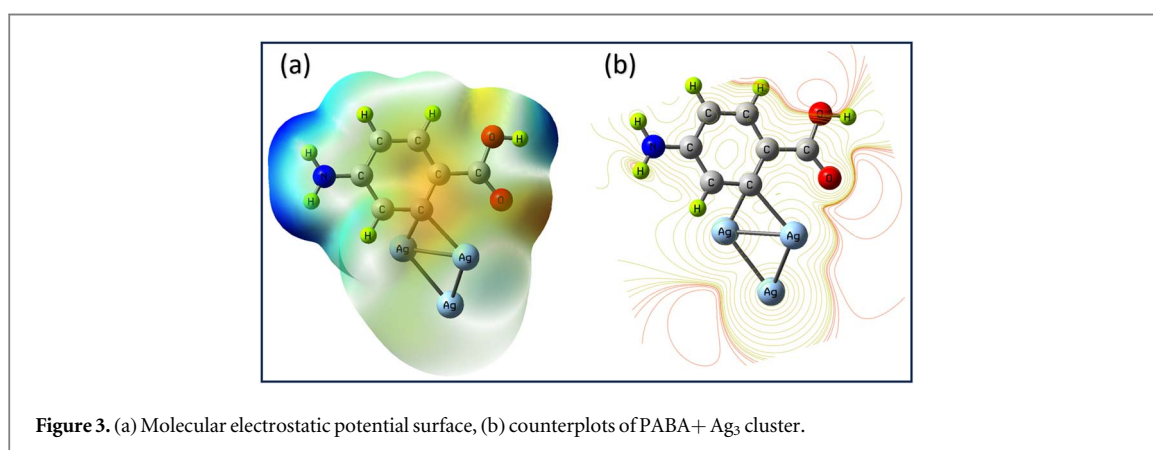
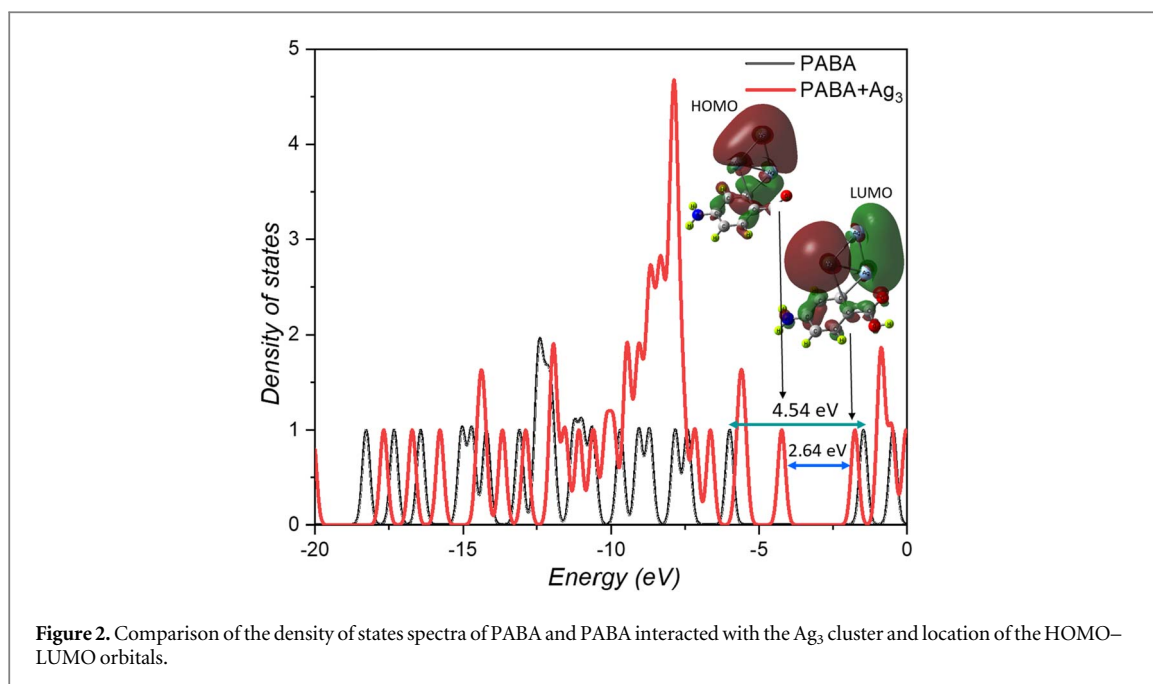
**Table 1.** Global reactivity parameters of probe PABA and PABA+Ag<sub>3</sub> complex (All values in eV and S is in (eV)<sup>-1</sup>).

Parameters	PABA	PABA+Ag <sub>3</sub> (Gas)	PABA+Ag <sub>3</sub> (Water)	PABA+Ag <sub>3</sub> (Methanol)	PABA+Ag <sub>3</sub> (DMF)	PABA+Ag <sub>3</sub> (DMSO)
HOMO	-5.964	-4.226	-4.307	-4.312	-4.312	-4.310
LUMO	-1.189	-1.748	-1.121	-1.134	-1.131	-1.126
ΔE	4.775	2.478	3.186	3.178	3.181	3.184
IP	5.964	4.226	4.307	4.312	4.312	4.310
EA	1.189	1.748	1.121	1.134	1.131	1.126
CP	-3.576	-2.987	-2.714	-2.723	-2.721	-2.718
χ	3.576	2.987	2.714	2.723	2.721	2.718
η	2.387	1.239	1.593	1.589	1.59	1.592
S	0.418	0.807	0.627	0.629	0.62	0.628

reduced after the introduction of the Ag<sub>3</sub> trimer. The calculated value of the band gap of the complex was found to be 2.478 eV. The significant reduction in the band gap of the complex in gas phase was due to the high chemical reactivity of the trimer. The band gap of complex in solvents water, methanol, DMF, and DMSO was calculated as 3.186, 3.178, 3.181, and 3.184 eV. After the optimization, it was found that the bond length associated with the trimer was large as compared to the rest of the bond length of PABA. The large bond lengths justify the easy generation of the charge cloud. A decrement in the band gap shows the easy excitation of the free charge for creating favourable conditions of intramolecular as well as intermolecular interactions. The value of IP (2.478 eV) in gas was also seen to decrease which shows the easy donating of the charge cloud via nucleophile of the complex. The value of IP in all the solvents was higher than that of the complex in gas phase. The EA seems to increase for the complex i.e., 1.189 eV to 1.748 eV. The EA is the energy that is required for withdrawing the charge cloud for the intramolecular interactions. The more the EA is, the more will be the chances of the availability of the charge cloud [37]. But, the value of EA in the considered solvents was less as compared to the gas phase. The CP is the potential that a molecule has for the intra and intermolecular charge association [38]. The more negative value of CP shows the chemical activity of the complex as compared to the probe PABA. χ is the tendency of atoms of a group of atoms to attract electrons toward them. The lower the electronegativity is, the higher will be the chemical reactivity of the considered complex as the lowest value of χ, a lower amount of energy is required for attracting the electrons and giving enhancement in the chemical reactivity [39]. For solvents this value was further reduced to 2.714 eV (water), 2.723 eV (methanol), 2.721 eV (DMF) and 2.718 eV (DMSO). The chemical hardness of the complex was reduced and softness increased due to the involvement of the nanoclusters. Moreover, the value of hardness of the complex increases in the presence of the solvents and the softness decreases in the solvents. The bonds of the nanoclusters were of long bond length resulting in the flexibility of the structures. Therefore, the chemical reactivity parameters analysis shows the occurrence of intramolecular and intermolecular interactions within the PABA singularly and amongst PABA and Ag<sub>3</sub> trimer. The density of state spectra (figure 2) was further obtained by computational means to verify the transportation of the charge cloud. The band gap obtained by DOS spectra (2.64 eV) was found nearly equal to that found using Koopman's identity (2.478 eV). This can be interpreted as the experimental studies done for the title complex will probably give a bad gap in the computational range. For predicting the dislocation of the charge cloud, the highest occupied and lowest unoccupied molecular orbital (HOMO–LUMO) surfaces were plotted and illustrated in figure 2. The green colored-charge surfaces were seen to dislocate from the Ag<sub>3</sub> nanocage towards the -COOH group. This HOMO–LUMO surface dislocation clearly indicates the intermolecular charge transfer among PABA and Ag<sub>3</sub>.

### 3.3. Surfaces and counters

The MEP surface was obtained for the PABA+Ag<sub>3</sub> complex to identify the charged moieties of the complex. In simple words, the MEP surface indicated the regions of a group of atoms that strongly imparted in donating the charge cloud from the positive moieties (blue-colored surface) and withdrawing the charge cloud (red region) [40]. From the surface shown in figure 3(a), the amino group induces the positively charged surface (say blue) and the carboxyl group induces the negatively charged surface (say red). Similar kind involvement was seen in probe PABA in our previously done work, but interestingly the strong participation of the Ag<sub>3</sub> in the complex was also observable. A light blue-colored region was observed near the Ag<sub>3</sub> trimer. This shows that along with the amino group, Ag<sub>3</sub> also participated in the generation of the charge cloud and charge donation. The interpretation of the MEP surface was in better agreement with the structural interpretation of the complex. A similar kind of activity can be shown using counterplots (figure 3(b)). The highly accumulated red counter lines around the carboxyl group show the availability of charge cloud over the carboxyl group and the availability of



the green lines around the amino group and Ag<sub>3</sub> trimer. Therefore, the MEP surface and counterplots predict the involvement of the trimer in the intramolecular interactions.

### 3.4. Mulliken and natural charge analysis

The charge interactions within the PABA+Ag<sub>3</sub> complex were quantitatively explained using the Mulliken and natural charge distribution. Figure 4 shows the comparison between both kinds of charges associated with each atom. The distribution of the charges (whether contributing positively or negatively to the total charge of the system) in both kinds of charges was found to be similar. All the hydrogen atoms contributed positively to the total charge of the complex. The oxygen atoms 1O and 2O share their negative contribution to the total charge of the complex. 3 N also acts contributed negatively. The magnitude of the charges of atoms has been labelled in figure 4. A significant charge difference was observed among the atoms corresponding to the amino and carboxyl groups. The Ag atoms, however, impart positively as well as negatively. 17 Ag and 18 Ag have Mulliken charges of 0.187 e and 0.164 e and natural charges of 0.358 e and 0.304 e respectively. Apart from these two atoms, 19Ag gave a negative Mulliken charge of  $-0.09$  e and a natural charge of  $-0.094$  e. The observed charge variation was capable enough to show the occurrence of intramolecular charge interactions between the PABA and Ag<sub>3</sub> trimer. Second-order perturbation Theory Analysis of the Fock Matrix in natural bond orbital (NBO) basis was used to calculate the delocalization energy of the charge from one atom to another. The NBO calculations evaluate the total amount of charge that is shared between the donor–acceptor of the molecules [41]. The delocalization energy was calculated for all the donor–acceptor moieties and the pairs with the highest delocalization energy were listed in table 2. In probe PABA, the charge 4C, 3N, 1O, and 1O were observed as donors, and 2O-10C and 10C were observed as acceptor moieties. But in the case of the PABA+Ag<sub>3</sub> complex, all

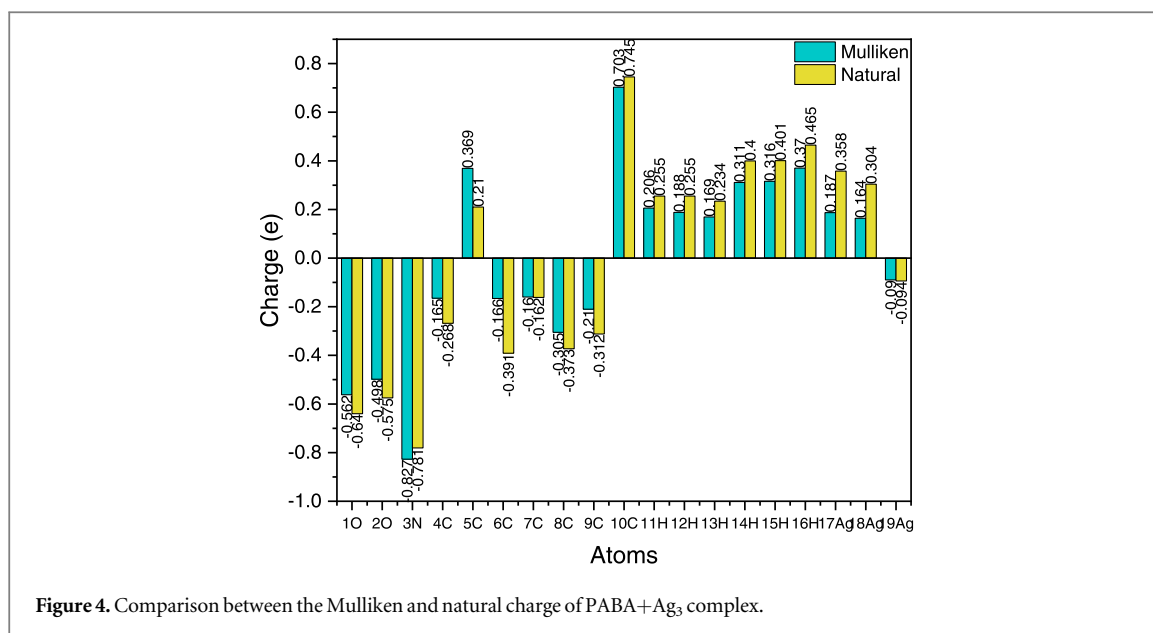


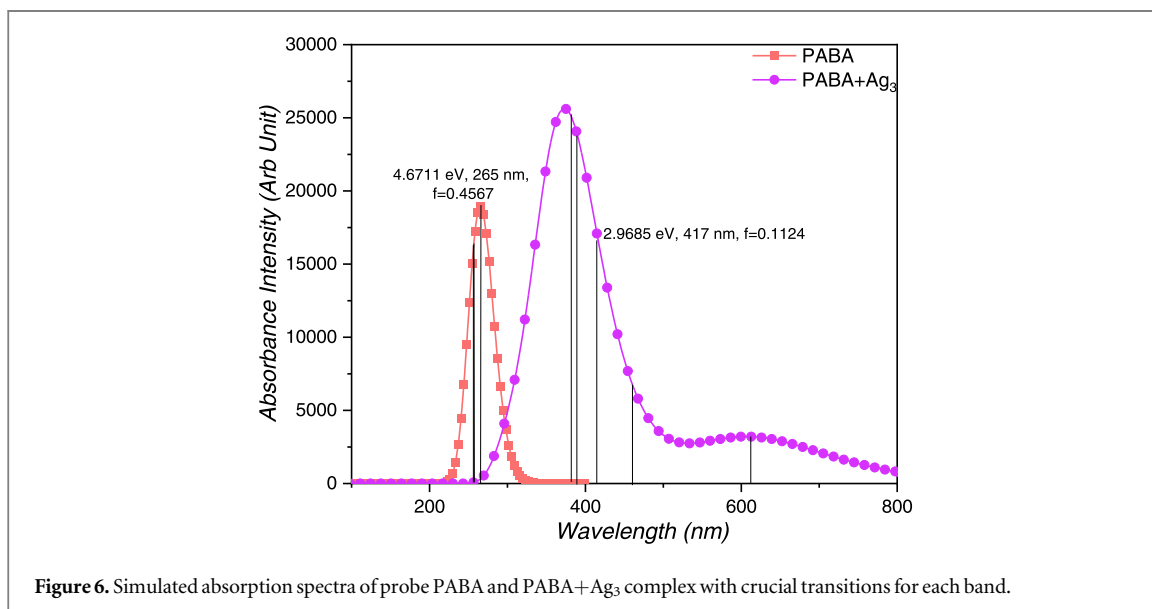
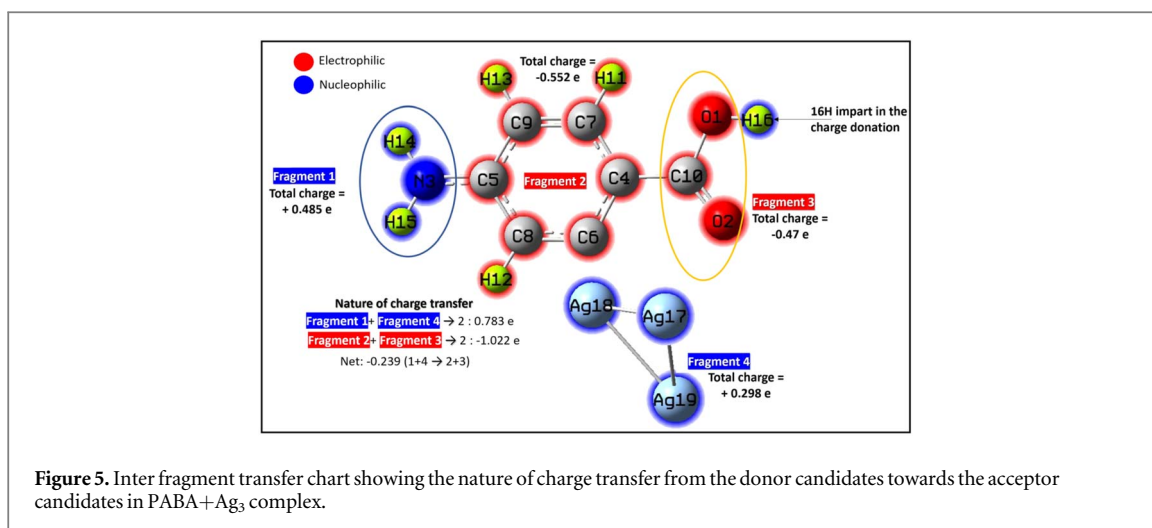
**Table 2.** Second-Order Perturbation Theory Analysis of Fock Matrix in NBO Basis of PABA and PABA+Ag<sub>3</sub> complex (LP- lone pair, LP\*- anti-bond lone pair, BD-bonding orbital, BD\*-antibonding orbital, CR-one core pair).

S. no.	Donor NBO ( <i>i</i> )	Acceptor NBO ( <i>j</i> )	$E(2)$ (kcal mol <sup>-1</sup> )	$E(j)-E(i)$ (au)	$F(i,j)$ (au)
<b>Within PABA</b>					
1.	LP (1) 4C	BD*(2) 2O-10C	142.88	0.08	0.109
2.	LP (1) 3 N	LP*(1) 5C	103.46	0.14	0.13
3.	LP (1) 1O	BD*(2) 2O-10C	52.68	0.28	0.114
4.	LP (1) 2O	RY*(1) 10C	12.56	1.59	0.128
<b>From PABA to Ag<sub>3</sub></b>					
1.	LP (1) 6C	LP*(6) 17Ag	47.36	0.19	0.087
2.	LP (1) 6C	LP*(6) 18Ag	17.35	0.33	0.073
3.	BD (1) 18Ag-19Ag	LP*(6) 17Ag	122.9	0.19	0.141

the Ag atoms were involved in charge donation. Thus, the NBO and charge transfer dislocation reveal the intramolecular charge interactions between PABA and Ag<sub>3</sub> trimer.

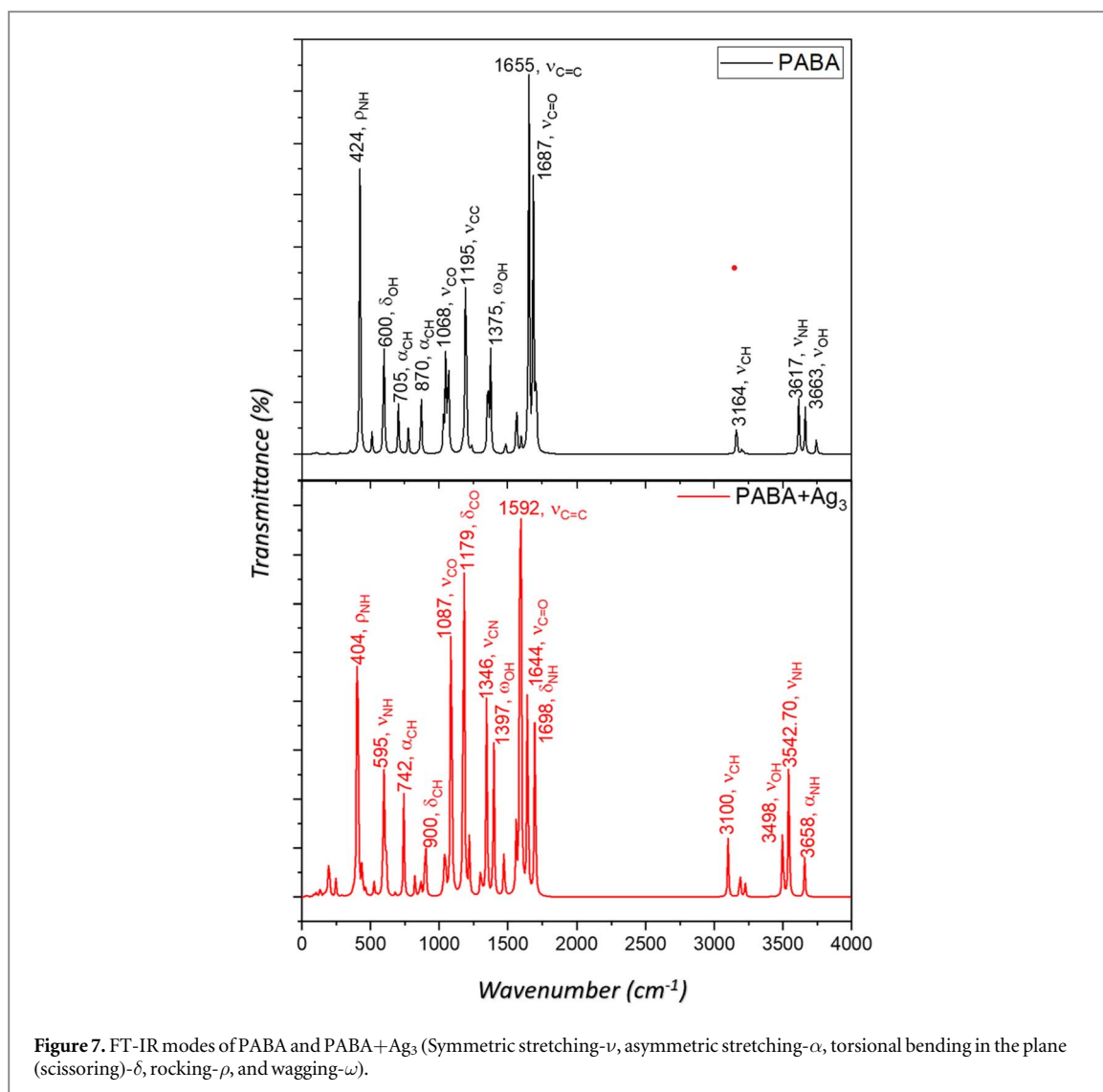
### 3.5. Inter-fragment charge transfer analysis

The inter-fragment charge transfer analysis is a quantitative approach to check specifically what amount of charge is shifted from donor to acceptor moieties [42, 43]. As per the nature of the region expressed by the MEP surface and the counterplot, the distribution of donor and acceptor candidates is highlighted in figure 5. The blue indication ensures the charge donation and the red surface ensures the charge withdrawal. The amino group (3N, 14H, 15H) and the Ag<sub>3</sub> trimer (17 Ag, 18 Ag, 19 Ag) behave as donors and are categorized as Fragment 1 and 4 respectively. The benzene ring (4C...9C, and 11H...13H) and the 1O, 2O, and 10C atoms of the carboxyl group act as acceptors and are fragment 2 and 3 respectively. In the MEP surface, a small blue kind of surface was visible over the 16H atom of the carboxyl group which indicates its contribution as a donor. The total natural charges corresponding to each fragment were obtained as +0.485 e, -0.552 e, -0.47 e, and +0.298 e for fragments 1, 2, 3, and 4 respectively. As there were two donor and two acceptor fragments, the total charge of the donor and acceptor was calculated by adding the total charge of fragments 1 and 4 for positive charge and fragments 2 and 3 for negative charge. By adding up the independent charges of each fragment, the total nucleophilic charge of fragment 1 + fragment 4 (+0.783 e) and the electrophilic charge of fragment 2 + fragment 3 (-1.022 e). The difference between the nucleophilic charge and electrophilic charge magnitude is referred to as the total charge that has been transferred from the donor to the acceptor moiety in the form of a charge cloud [44]. Therefore, 0.239 e is the amount of charge that has been transferred from the nucleophilic sites toward the electrophilic sites in the PABA+Ag<sub>3</sub> complex. The amount of charge that is being transferred in the PABA+Ag<sub>3</sub> complex is lower as compared to the transferred charge in the case of probe PABA i.e., 0.30 e [29]. This might be due to the involvement of the multiple nucleophilic and electrophilic sites in the PABA+Ag<sub>3</sub> complex as compared to the probe PABA.



### 3.6. Electronic properties

The electronic properties of the PABA+Ag<sub>3</sub> complex were studied using the absorption spectra. The absorption spectra were calculated using TD-DFT techniques for up to nine transitions. The absorption spectra of both probe PABA and complex are shown in figure 6. A wide absorption band of probe PABA was obtained between 200–400 nm with S<sub>0</sub>→S<sub>1</sub> transition at the highest wavelength of 365 nm oscillator strength of 0.4567 and excitation energy of 4.67 eV. The other transitions were observed around 240 nm and shown with black lines in the spectra. The absorption spectra of the PABA+Ag<sub>3</sub> complex were seen to experience a bathochromic shift in the range of 200–800 nm. A stretched absorption band with one with higher absorption intensity than that of the probe PABA and a stretched shoulder between 450–800 nm. The major transition with the highest oscillator strength of 0.1124 was observed at 417 nm. However, the sharp peak of the absorption of PABA+Ag<sub>3</sub> was observed around 390 nm. The drastic shift in the maximum absorption wavelength of the complex was due to the maximum absorption wavelength of Ag nanoparticles around 400 nm which was observed in a lot of experimental studies previously [45, 46]. Thus, taking the maximum wavelength of Ag nanoparticles into consideration, the Ag<sub>3</sub> trimer considered in the present study which has a maximum absorption wavelength of 417 nm can be considered as a nanoparticle. Although, the experimental validation of the reported study will be carried out in the future. The other transitions observed for the PABA+Ag<sub>3</sub> complex are indicated in the spectra using the black lines. Therefore, the adsorption of Ag<sub>3</sub> over the PABA results in the transition of free electrons from a bonding π orbital to an antibonding π\* orbital. Thus, the observed range of absorption wavelength indicates the π→π\* excitation of the electronic transitions in the PABA+Ag<sub>3</sub> complex [47]. The occurrence of



such transitions and significant red shift in the excitation wavelength shows the enhanced chemical reactivity of PABA after the adsorption of the Ag<sub>3</sub> trimer.

### 3.7. Vibrational properties

The prominent vibrational modes corresponding to the bonds of the complex were analyzed to check the response of the functional groups and chemically reactive sites toward the infrared radiation [48]. The comparison between the FT-IR spectra of probe PABA and PABA+Ag<sub>3</sub> complex is shown in figure 7. The silver trimer gave asymmetric and symmetric stretching at 133 and 180 cm<sup>-1</sup> respectively. These modes were not highly observed in the IR spectra. The FT-IR spectra mainly comprise the higher IR intensity modes for the functional groups (say amino and carboxyl groups in PABA). The only difference in the spectra of PABA and PABA+Ag<sub>3</sub> was the vibrational modes in the case of PABA+Ag<sub>3</sub> were seen to readily shift towards the lower IR radiation. This might be due to the introduction of the silver trimer. Moreover, the FT-IR of the complex was beneficial in predicting the available functional groups in the complex and checking the suitable location for the silver trimer to get adsorbed onto the surface of PABA. The major modes for the vibrations of functional groups like  $\rho_{\text{NH}}$  and  $\delta_{\text{OH}}$  were observed to shift from 424 and 600 to 404 and 595 cm<sup>-1</sup> respectively. Along with these modes, all the other prominent vibrational modes were shifted toward the lower wavenumbers. The  $\nu_{\text{C=C}}$  mode was observed at 1655 cm<sup>-1</sup> in PABA and 1592 cm<sup>-1</sup> in the complex. This was the mode with the highest IR intensity. This mode corresponds to the stretching of the 8C–6C mode. This was a favorable site for the silver trimer to get interact with. The symmetric stretching ( $\nu$ ), torsional bending ( $\delta$ ), and asymmetric stretching of the amino group were observed at 595, 1698, and 3658 cm<sup>-1</sup> respectively. The rest of the important modes can be seen from the FT-IR spectra. Therefore, the FT-IR helps us to identify the adsorption site and the confirmation of the functional groups in the PABA+Ag<sub>3</sub> complex.

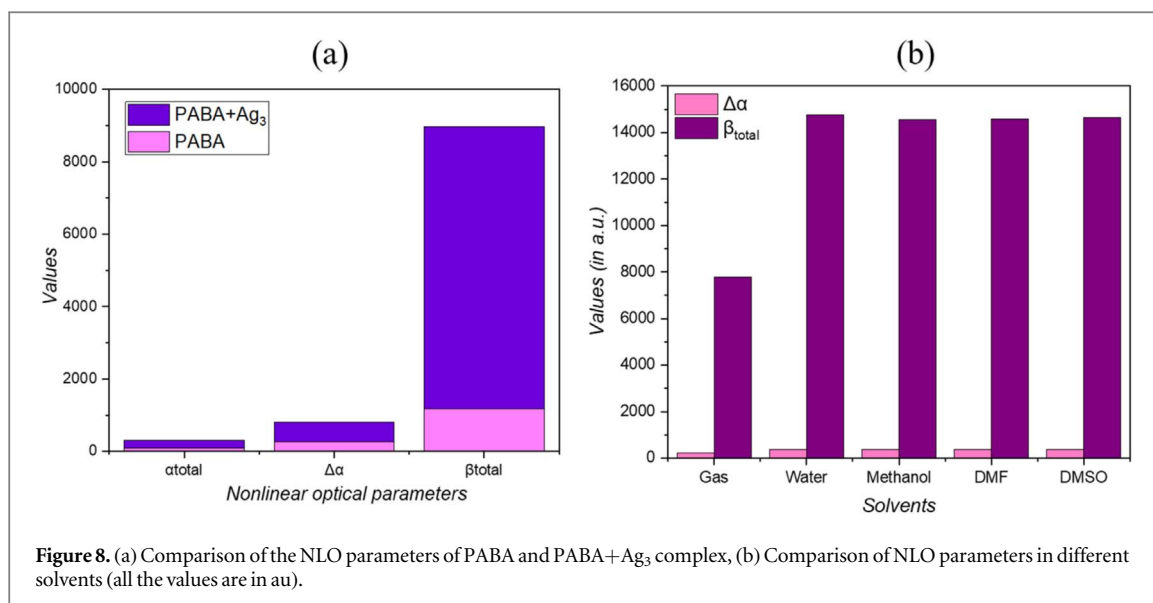


**Figure 8.** (a) Comparison of the NLO parameters of PABA and PABA+Ag<sub>3</sub> complex, (b) Comparison of NLO parameters in different solvents (all the values are in au).

**Table 3.** Values of the NLO parameters of the PABA+Ag<sub>3</sub> complex in different solvents.

Solvents	$\alpha_{total}$	$\beta_{total}$
Gas	224.52	7782.85
Water	382.126	14769.05
Methanol	372.67	14545.83
DMF	374.59	14590.86
DMSO	377.49	14657.17

All the values are in au.

### 3.8. Nonlinear optical responses

The NLO parameters like dipole moment ( $\mu_{total}$ ), isotropic polarizability ( $\alpha_{total}$ ), anisotropic polarizability ( $\Delta\alpha$ ), and first-order hyperpolarizability ( $\beta_{total}$ ) are used by the researchers for computationally predicting the optical nonlinearity of the compounds (figure 8).  $\mu_{total}$  is the virtue of the compounds that reveals the net polarity of the compounds. Compounds with large electronegativity differences between their elemental composition create a rise in the  $\mu_{total}$  [49]. The high  $\mu_{total}$  leads to high polarizability and shows strong candidature of the compounds as a medium for optical nonlinearity. The dipole moment for both PABA and PABA+Ag<sub>3</sub> complex was high. The  $\alpha_{total}$  is a quantitative measure of the isotropy of the compounds. Compounds that have uniform distribution of the atoms in all directions or have uniform properties in all directions are centrosymmetric in nature and have higher values of  $\alpha_{total}$  whereas the non-centrosymmetric compounds have different properties in different directions and thus have higher values for  $\Delta\alpha$  [50]. The lower value of  $\alpha_{total}$  as compared to  $\Delta\alpha$  was obtained for both PABA and PABA+Ag<sub>3</sub>. The introduction of the solvent gave rise to the value of  $\alpha_{total}$  for PABA+Ag<sub>3</sub>. The values of  $\alpha_{total}$  for solvents water, methanol, DMF, and DMSO were computed as 382.186, 372.67, 374.59, and 377.49 au respectively. The  $\Delta\alpha$  was seen to rise to 540.53 au rather than 270.7 au after the introduction of the Ag<sub>3</sub> nanoparticle. Thus, the value of  $\Delta\alpha$  for PABA+Ag<sub>3</sub> rises to double. These parameters are the higher-order coefficients of the electric field terms in the expansion of the polarizability when the field is high in intensity and the material behaves nonlinearly. The  $\alpha_{total}$  and  $\Delta\alpha$  are lower order coefficients and help in the identification of the nature of properties, whereas  $\beta_{total}$  is the higher order coefficient and shows the optical nonlinearity of the compound. The value of  $\beta_{total}$  is elevated from 1185.22 au for PABA to 7782.85 au for PABA+Ag<sub>3</sub>. A higher value of  $\beta_{total}$  shows the enhanced NLO activity of the PABA+Ag<sub>3</sub> complex as well. For solvents water, methanol, DMF, and DMSO, the value of  $\beta_{total}$  was observed as 14769, 14545, 14590, and 14657 au respectively. Figure 8(b) shows the comparison between the NLO parameters of the complex in different mediums and the values of the NLO parameters in the solvents have been listed in table 3. The values of  $\beta_{total}$  in solvents were higher than that of the complex in the gas medium. Thus, the higher value of  $\beta_{total}$  in solvents supports the higher NLO responses of the proposed complex in the

solvents as well and water can be considered as the best medium for making the solution of the proposed complex.

#### 4. Conclusion

The present study is the computational study performed for the PABA after the adsorption of the silver nanoparticle in the form of trimer  $\text{Ag}_3$ . Previously we have done experimental verification on the NLO activity and optical limiting of PABA alone and got satisfying results. Along, with some of our previously done studies we found that  $\text{Ag}_3$  acts as the best dopant for increasing the NLO activity of the probe organic systems. The structural analysis shows the adsorption of the silver nanoparticle over the benzene ring and the charge transfer established the occurrence of the intramolecular charge transfer within the PABA and trimer. The quantitative approach shows a total of 0.239 e charge has been transferred between the donor (amino and trimer) and acceptors (carboxyl and benzene). Absorption spectra with bathochromic shift and higher intensity were obtained for the PABA+ $\text{Ag}_3$  complex which suggests the  $\pi \rightarrow \pi^*$  nature of the transitions. The higher value of anisotropic polarizability and first-order hyperpolarizability PABA+ $\text{Ag}_3$  complex as compared to probe PABA suggests that the doping/introduction of the silver nanoparticles can give better values for the NLO parameters and the experimental study can further be performed for the title complex without any bias. Therefore, the analysis suggests the strong candidature of the PABA+ $\text{Ag}_3$  complex in many NLO applications.

#### Data availability statement

The data cannot be made publicly available upon publication because no suitable repository exists for hosting data in this field of study. The data that support the findings of this study are available upon reasonable request from the authors.

#### Declarations

#### Ethical approval

This material is the author's original work, which has not been previously published elsewhere. All authors have been personally and actively involved in substantial work leading to the paper and will take public responsibility for its content. The paper properly credits the meaningful contributions of all the co-authors.

#### Competing interests

The authors declare that they have no known competing financial interests or personal relationships that could have appeared to influence the work reported in this paper.

#### Authors' contributions

Shradha Lakhera: Data curation, Writing-Original draft preparation, Visualization, Investigation, Software, Validation.

Meenakshi Rana: Conceptualization, Methodology, Writing-Reviewing and Editing, Supervision.

Kamal Devlal: Conceptualization, Writing- Reviewing and Editing.

#### Funding

S. Lakhera and M. Rana thank Uttarakhand Science Education and Research Centre (USERC), Department of Information and Science Technology, Government of Uttarakhand, for financial support through an R&D Research Project (Project no: USERC/2023-24/190).

## Availability of data and materials

All data generated or analyzed during this study, which support the plots within this paper and the other findings of this study, are included in this article and its Supplementary Information. Source data are provided in this paper.

## ORCID iDs

Meenakshi Rana  <https://orcid.org/0000-0002-9156-9125>

## References

- [1] Mary Y S, Bolelli T E, Thomas R, Krishnan A R, Bolelli K, Kasap E N, Onkol T and Yildiz I 2019 Quantum mechanical studies of three aromatic halogen-substituted bioactive sulfonamidobenzoxazole compounds with potential light-harvesting properties *Polycycl Aromat Compd.* **41** 1563–79
- [2] Rana M, Singla N, Pathak A, Dhanya R, Narayana C and Chowdhury P 2017 Vibrational-electronic properties of intra/inter molecular hydrogen bonded heterocyclic dimer: an experimental and theoretical study of pyrrole-2-carboxaldehyde *Vib. Spectrosc.* **89** 16–25
- [3] Felscia U R, Rajkumar B J M and Mary M B 2018 Charge transport properties of pyrene and its derivatives: optoelectronic and nonlinear optical applications *J. Mater. Sci.* **53** 15213–25
- [4] More A B and Sekar N 2017 Nonlinear optical properties of pyrene based fluorescent hemicurcuminoid and their BF<sub>2</sub> complexes – spectroscopic and DFT studies *J. Fluoresc.* **27** 1777–92
- [5] Saral A, Sudha P, Muthu S, Sevvanthi S and Irfan A 2022 Molecular structure spectroscopic elucidation, IEFPCM solvation (UV–Vis, MEP, FMO, NBO, NLO), molecular docking and biological assessment studies of lepidine (4-Methylquinoline) *J. Mol. Liq.* **345** 118249
- [6] Irudaya Jothi A, Wilson Bosco Paul M and Alexander V 2022 A comparative molecular structure—NLO activity study of ortho-bridged dibenzaldehydes: Synthesis, crystal structure, SHG, and DFT studies *J. Mol. Struct.* **1250** 131776
- [7] Lakhera S, Devlal K, Ghosh A and Rana M 2022 Modelling the DFT structural and reactivity study of feverfew and evaluation of its potential antiviral activity against COVID-19 using molecular docking and MD simulations *Chem. Pap.* **76** 2759–76
- [8] Runowski M, Marcinkowski D, Carracedo K S, Gorczyński A, Ewert E, Woźny P and Martín I R 2023 Noncentrosymmetric lanthanide-Based MOF materials exhibiting strong SHG activity and NIR luminescence of Er<sup>3+</sup>: application in nonlinear optical thermometry *ACS Appl. Mater. Interfaces* **15** 3244–52
- [9] Kusaka R and Watanabe M 2022 Development of heavy element chemistry at interfaces: observing actinide complexes at the oil/water interface in solvent extraction by nonlinear vibrational spectroscopy *J. Phys. Chem. Lett.* **13** 7065–71
- [10] Bajaj I K, Guzauskas M, Janusik M M, Zagórska M, Mahmoudi M, Grazulevicius J V, Proń A and Volyniuk D 2022 Acridone and quinacridone derivatives with carbazole or phenoxazine substituents: synthesis, electrochemistry, photophysics and application as TADF electroluminescence *J. Mater. Chem. C* **10** 12377–91
- [11] Ray P C 2010 Size and shape dependent second order nonlinear optical properties of Nanomaterials and their applications in biological and chemical sensing *Chem. Rev.* **110** 5332–65
- [12] Gouadec G and Colombari P 2007 Raman spectroscopy of nanomaterials: how spectra relate to disorder, particle size and mechanical properties *Prog. Cryst.* **53** 1–56
- [13] Inah B E, Louis H, Benjamin I, Unimuke T O and Adeyinka A S 2022 Computational study on the interactions of functionalized C<sub>24</sub>NC (NC=C, –OH, –NH<sub>2</sub>, –COOH, and B) with chloroethylphenylbutanoic acid *Can. J. Chem.* **101** 11–24
- [14] Beltrán G G, Zúñiga C M, SanMiguel C R T, García G G and Torres C T 2022 Photonic encryption by optical activity in Kerr-like carbon-based nanofluids with plasmonic nanoparticles *J. Mol. Liq.* **367** 120424
- [15] Ghazy A R, Shalaby M G, Ibrahim A, ElShaer A, Mahmoud Y A G and Al-Hossainy A F 2022 Synthesis, structural and optical properties of Fungal biosynthesized Cu<sub>2</sub>O nanoparticles doped Poly methyl methacrylate-co-Acrylonitrile copolymer nanocomposite films using experimental data and TD-DFT/DMO3 computations *J. Mol. Struct.* **1269** 133776
- [16] Sichao D et al Auger scattering dynamic of photo-excited hot carriers in nano-graphite film *Appl. Phys. Lett.* **121** 1811047
- [17] Zhao Q, Liu J, Yang H, Liu H, Zeng G and Huang B 2022 High birefringence D-shaped germanium-doped photonic crystal fiber sensor *Micromachines* **13** 826
- [18] Song Z, Han D, Yang M, Huang J, Shao X and Li H 2023 Formic acid formation via direct hydration reaction (CO + H<sub>2</sub>O → HCOOH) on magnesia-silver composite *Appl. Surf. Sci.* **607** 155067
- [19] Chen P B, Yang J W, Rao Z X, Wang Q, Tang H T, Pan Y M and Liang Y 2023 Efficient *in situ* conversion of low-concentration carbon dioxide in exhaust gas using silver nanoparticles in N-heterocyclic carbene polymer *J. Colloid Interface Sci.* **652** 866–77
- [20] John J S, Sajan D, Narayana C and Sundius T 2018 Optical nonlinearity and charge transfer analysis of 4-[(E)-2-(2,4,6-Trinitrophenyl) ethylidene] benzonitrile adsorbed on silver nanoparticles: computational and experimental investigations *Opt. Laser Technol.* **107** 454–67
- [21] John J S, Sajan D, Prabukanthan P, Philip R and Joy N 2019 Enhanced NLO activity of organic 2-methyl-5-nitroaniline crystal: experimental and computational investigation with and without silver addition *Opt. Laser Technol.* **113** 416–27
- [22] Reeta Felscia U, Rajkumar B J M, Sankar P, Philip R and Briget Mary M 2017 Optical nonlinearity and charge transfer analysis of pyrene adsorbed on silver: Computational and experimental investigations *Spectrochim. Acta - A: Mol. Biomol. Spectrosc.* **184** 286–93
- [23] John J S and Sajan D 2020 Computational analysis of vibrational spectroscopic properties and hyperpolarizability of silver adsorbed organic molecule, N, N' Dimethyl Urea Ninhydrin *Spectrochim. Acta - A: Mol. Biomol. Spectrosc.* **228** 117698
- [24] Reeta Felscia U, Rajkumar B J M, Nidya M and Sankar P 2018 Electronic and nonlinear optical properties of l-histidine on silver: a theoretical and experimental approach *J. Phys. Chem. A* **122** 1045–52
- [25] Aboalhassan A A et al 2022 Plasmonic surface of metallic gold and silver nanoparticles induced fluorescence quenching of Meso-Terakis (4-Sulfonatophenyl) Porphyrin (TPPS) and theoretical–experimental comparable *J. Fluoresc.* **32** 2257–69
- [26] Lakhera S, Rana M and Devlal K 2023 Influence of adsorption of gold and silver nanoclusters on structural, electronic, and nonlinear optical properties of Pentacene-5, 12-dione: A DFT study *Opt Quant Electron.* **55** 178
- [27] Lakhera S, Devlal K, Rana M, Dhuliya V and Pandey N 2023 Non-linear optical behavior of 2,9-dimethylquinacridone with adsorbed gold and silver nanoclusters *Optik* **286** 170983

- [28] González Fá A, Pignanelli F, López-Corral I, Faccio R, Juan A and Nezio M S D 2019 Detection of Oxytetracycline in honey using SERS on silver nanoparticles *Trends in Analytical Chemistry* **121** 115673
- [29] Lakhera S, Rana M, Devlal K, Sharma S, Chowdhury P, Dhuliya V, Panwar S, Purohit S L P, Dhanusha A and Girisun T C 2023 Exploring the Nonlinear optical limiting activity of para-aminobenzoic acid by experimental and Dft approach *J. Photochem. Photobiol., A* **444** 114987
- [30] Frisch M J 2010 *Gaussian 09, Revision B.01* (Gaussian Inc.)
- [31] Becke A D 1993 Density-functional thermochemistry. III. The role of exact exchange *J. Chem. Phys.* **98** 5648
- [32] Becke A D 1997 Density-functional thermochemistry. V. Systematic optimization of exchange-correlation functionals *J. Chem. Phys.* **107** 8554–60
- [33] Koopmans T 1934 About the assignment of wave functions and eigenvalues for the individual electrons in an atom *Physica* **1** 104–13
- [34] Lakhera S, Rana M and Devlal K 2023 Investigation of nonlinear optical responses of organic derivative of imidazole: imidazole-2-carboxaldehyde *IJMR*. **114**
- [35] Lakhera S, Rana M, Devlal K, Kanagathara N and Janczak J 2023 Photovoltaic characteristics of organic heterocyclic 2,9-dimethyl quinacridone in different solvents using DFT approach *J. Photochem. Photobiol., A* **114664** 1010–6030
- [36] Yanxin Y, Yulin H, Pan L, Hui Z, Qiuying Z, Jialiang L, Linghan X, Xibin W, Yuhui A and Ming L 2021 Mild and *in situ* photocrosslinking of anthracene-functionalized poly (aryl ether ketone) for enhancing temporal stability of organic NLO materials *J. Mater. Sci.* **56** 5910–23
- [37] Ojo N D, Krause R W and Egbedi N O O 2020 Electronic and nonlinear optical properties of 2-(((5-aminonaphthalen-1-yl)imino) methyl)phenol: Experimental and time-dependent density functional studies *J. Mol. Liq.* **319** 114157
- [38] Lakhera S, Devlal K, Rana M and Celik I 2022 Study of nonlinear optical responses of phytochemicals of *Clitoria ternatea* by quantum mechanical approach and investigation of their anti-Alzheimer activity with *in silico* approach *Struct. Chem.* **34** 439–54
- [39] Felscia U R, Rajkumar B J M and Mary M B 2018 Theoretical investigations on nonlinear fused 4-ring systems: Application to OLED and NLO devices *Synth. Met.* **246** 31–8
- [40] Lakhera S, Devlal K, Rana M and Dhuliya V 2022 Quantum mechanical study of three aromatic bioactive fatty alcohol compounds with nonlinear optical and potential light harvesting properties *Opt. Mater.* **129** 112476
- [41] Rana M, Chatterjee A and Chowdhury P 2018 Investigation of nonlinear optical properties of organic based di amine substituted tetraphenylethylene *AIP Conf. Proc.* **2009** 020055
- [42] Lakhera S, Rana M and Devlal K 2022 Theoretical study on spectral and optical properties of essential amino acids: a comparative study *Opt. Quantum Electron.* **54** 714
- [43] Weeraratna C, Amarasinghe C, Lu W and Ahmed M 2021 A direct probe of the hydrogen bond network in aqueous glycerol aerosols *The Journal of Physical Chemistry Letters, J. Phys. Chem. Lett.* **12** 5503–11
- [44] Karatay A et al 2022 Amino-functionalized nitrogen-doped graphene quantum dots and silver-graphene based nanocomposites: Ultrafast charge transfer and a proof-of-concept study for bioimaging applications *J. Photochem. Photobiol. A* **426** 113741
- [45] Tessa C B N et al 2022 DFT investigation on the effect of the permutation of some electron donating and accepting groups in the charge transfer process within 2-((E)-[2-hydroxyphenyl]imino) methyl)phenol *Theor. Chem. Acc.* **141** 31
- [46] Yildiz E A et al 2023 Effects of heavy iodine atoms and  $\pi$ -expanded conjugation on charge transfer dynamics in carboxylic acid BODIPY derivatives as triplet photosensitizers *Chem. Phys. Chem.* **24** e202200735
- [47] Johna J S, Sajana D, Prabukanthanb P, Philipc R and Joyc N 2019 Enhanced NLO activity of organic 2-methyl-5-nitroaniline crystal: Experimental and computational investigation with and without silver *Opt. Laser Technol.* **113** 416–27 addition
- [48] Chen Y et al 2021 Improved optical properties of perovskite solar cells by introducing Ag nanoparticles and ITO AR layers *Sci Rep.* **11** 14550
- [49] Lakhera S, Devlal K, Rana M and Dhuliya V 2023 Computational study of non-linear optical and electrical properties of 1,3-dinitropyrene *Opt Quant Electron.* **55** 85
- [50] Lakhera S, Rana M and Devlal K K 2023 Investigation of the electronic and optical activity of halogen-substituted 2-nitrotoulene by density functional theory *Opt Quant Electron.* **55** 292